

No-load electromagnetic simulations of a hydropower generator considering the effect of rotor whirling

Y. Calleecharan, J.O. Aidanpää, and J.R. Brauer, *Life Fellow IEEE*

Abstract—Electromagnetic (EM) analysis of hydropower generators is common practice but there is little emphasis on studying the effect of rotor whirling in the analysis. This paper explores the effect on electromagnetic analysis as the rotor is allowed to whirl both in forward and in backward directions under no-load conditions. As a hydropower generator rotor shaft can experience whirling when under eccentric operation, the objective is to examine how whirling can affect the unbalanced magnetic pull (UMP), flux densities, damper currents, and ohmic losses in a synchronous hydropower generator. These results are obtained in a commercial FEM-based EM field modelling software package that allows various degrees of freedom in motion types and multiple motion components to be set. It is seen that backward whirling tends to induce higher eddy currents than forward whirling does.

Index Terms—eccentricity, electromagnetic simulations, hydropower rotor, no-load, whirl

NOMENCLATURE

Γ	domain boundary
μ	magnetic permeability [H/m]
σ	electrical conductivity [S/m]
ρ_V	charge density [C/m ³]
ω	angular velocity [rad/s]
Ω	domain
∇	differential operator
\mathbf{A}	magnetic vector potential [T m = Wb/m]
\mathbf{B}	magnetic flux density [T]
\mathbf{D}	electric flux density [C/m ²]
\mathbf{E}	electric field strength [V/m]
f	frequency in linear spectrum estimation [Hz]
F	Force [N]
\mathbf{H}	magnetic field strength [A/m]
\mathbf{J}	current density [A/m ²]
l	frequency index in linear spectrum estimation
n	time index in linear spectrum estimation
N	positive integer number
t	time [s]
U	window-dependent resolution bandwidth normalisation factor
UMP	unbalanced magnetic pull [N]
\mathbf{v}	velocity [m/s]
w	data window
\hat{X}	one-sided linear spectrum estimate

Y. CALLEECHARAN is with the Department of Mechanical and Production Engineering, University of Mauritius, Réduit, 80837, Mauritius (email: y.calleecharan@uom.ac.mu).

J.O. AIDANPÄÄ is with the Department of Engineering Sciences and Mathematics, Luleå Tekniska Universitet, Luleå, 971 87, Sweden (email: joa@ltu.se).

J.R. BRAUER is with the Department of Electrical Engineering and Computer Science, Milwaukee School of Engineering, Milwaukee, Wisconsin, 53202, USA (email: jbrauer@ieee.org).

subscripts & superscripts

ro	rotor
s	sampling
wh	whirl
whr	whirl ratio
0	impressed current
c	conducting
n	non-conducting
LS	linear spectrum

I. INTRODUCTION

ROTOR-stator eccentricity in electrical machines is an issue that has caught attention for a long time [1], [2] and is an important item in condition monitoring [3] in electrical machines. Though many papers in the literature [4]–[8] have addressed the issue of eccentricity in rotating electrical machines, there has been a paucity of papers that account for the effect of whirling of the rotor. Examples of publications that have considered whirling include [9], [10].

Rotor whirling in hydropower machines is not uncommon [11]. Whirling motion is associated with any eccentric motion of the rotor where the geometric centre of the rotor does not coincide with the axis of rotation of the rotor. In a two-dimensional setting neglecting mass eccentricity effects, we may say that a whirl velocity component only exists between two points when there is relative motion between them. The simplest form of whirling thus occurs with a purely dynamic eccentricity motion and the latter is discussed in the next section. Whirling in a hydropower rotor can occur apart from unbalance effects because of, for example, play in bearings, the pulling effect of the UMP and also water forces hitting the turbines' blades that can aggravate any pre-existing play in the bearings supporting the rotor. While backward whirling of a rotor is considered to occur less commonly in practice, the electromagnetic (EM) simulations in the present paper aims to investigate the effects of both forward (positive direction) and backward (negative direction) motion types of the rotor. It has been found that many FEM-based EM field modelling software packages cannot handle dynamic eccentricity motion, and worse a combination of static and dynamic eccentricities motion. The latter motion combination is more amenable to model what actually happens in a hydropower machine but will not be discussed in this paper. A large majority of existing FEM-based EM software products cannot handle eccentricity cases and have made no provisions for the user to be able to add whirling effects since there can be perhaps only very little demand from users to simulate whirling behaviour. And it turns out that the main users of these FEM-based EM software packages are electrical machine designers whose primary interests rest in the electrical characteristics of a machine rather in their electromechanical aspects.

Previous works [12], [13] carried out by two of the authors have had goals to examine the rotor movements and the stability of an industrial hydropower generator under a purely dynamic eccentricity motion. These two papers however only emphasised the importance of whirling as a mechanical issue and not as an electromechanical one. The present paper takes a step back and investigates what useful

information can be gained rather directly from the field solutions in the EM analysis, and indirectly from post-processed results in the software package under zero eccentricity condition, a purely static eccentricity condition, and finally a purely dynamic eccentricity condition. In a future work, it is hoped that a more electromechanical approach can thus be undertaken whereby EM field solutions and post-processed results can be linked seamlessly with a mechanical analysis.

The simulations in this article furthermore demonstrate the capabilities of one FEM-based EM field modelling software product. There is a need to motivate electrical machine designers on the need to consider whirling of the rotor when designing hydropower generators as whirling effects occur in reality. Thus to aid the machine designers, information on the EM field solutions such as the flux densities and ohmic losses are provided in addition to current waveforms, and forces (unbalanced magnetic pull) due to eccentricity effects or asymmetry in flux distribution around the rotor. This information will normally complement a dynamic analysis of the generator. Examples of dynamic analyses for a generator considering both the range of forward and backward whirls, and where a purely dynamic eccentricity motion exists are given in [12], [13].

Present models in the hydropower industry in Sweden use only a single value of the unbalanced magnetic pull (UMP) (see e.g. [12]). Though this UMP value tells us the maximum radial force (at synchronous rotor whirl) and hence the maximum force acting between the rotor and the stator given that the radial force is normally greater than the tangential component, relying upon this single value estimate can be misleading as was shown in [12], [13]. This is because the whirling frequency of the rotor is changing all the time when the generator is under operation in an actual hydropower machine, and one has to consider the effect of both the radial and the tangential forces then so as to grasp the dynamics of the machine. Hence the present paper also comes in as a step to strengthen the fact that a complete EM analysis of a hydropower generator needs consideration of the whirling frequency of the rotor both in the positive and in the negative whirl directions.

A small-scale synchronous generator [14] which has been specially made available for hydropower research is used in this study. Measurements have not been performed by the authors. However, it is mentioned in Section IV-A that an experimental measurement of the force or the UMP was carried out by Uppsala Universitet [14] on a static eccentricity motion case. Simulations and analysis by the present authors have then become possible after the FEM-based software package used in the present paper reported in a corresponding static eccentricity simulation a UMP magnitude value comparable to that obtained in the experimental measurement.

There is also a caveat in doing proper eccentricity measurements in an experimental setup. If one is able to set up a desired purely static eccentricity or a purely dynamic eccentricity on a rotor, it is to be realised that when the generator is put in service, then any UMP that arises because of the eccentricity or because of any other reason that leads to an asymmetric distribution of flux around the rotor will affect the eccentricity value set by the experimenter on the rotor. This implies that the eccentricity at which one is doing the measurement will change value, making the measurement of the UMP in practice rather an impossible task at the given fixed eccentricity setting of the rotor that is set and sought by the experimenter.

II. CLARIFICATION OF STUDIED ECCENTRICITY TYPES

Two types of eccentricities in a two-dimensional setting are considered in this article, namely purely static eccentricity and purely dynamic eccentricity. Mixed eccentricities, whereby both types of eccentricities are present, are not within the scope of the present study

though in practice separating a mixture of these two types of eccentricities can be an impossible task. It is to be reminded that an actual generator rotor motion is inclined to embrace a mixed eccentricities motion in practice. Also, eccentricities that involve offset of the stator bore centre or simultaneous offset of the former together with offset of the rotor centre are not treated in this paper. The two types of eccentricities are shown in Fig. 1. It is to be noted that though a static eccentricity in the positive Cartesian x -direction (see Fig. 1a) has been studied in this article, eccentricities in other Cartesian directions (positive and negative) have as similar corresponding behaviours as that displayed by the considered positive x -direction eccentricity.

In the case of a purely static eccentricity in the positive Cartesian x -direction which is shown in Fig. 1a, the axis of rotation of the rotor (marked as x in the figure) and the geometric centre of the rotor (marked as o) coincide with each other, and are at an eccentric distance in the positive x -direction from the geometric centre of the stator bore (marked as $+$). Put in another words, for a static eccentricity in the positive x -direction, the geometric centre of the rotor is displaced by x_s in the positive x -direction from the geometric centre of the stator bore. Since the geometric centre of the rotor coincides with the axis of rotation of the rotor based on the sound assumption that there is usually no unbalance in the rotor, the axis of rotation of the rotor is also displaced by the vector $(x_s, 0)$ from the stator bore centre.

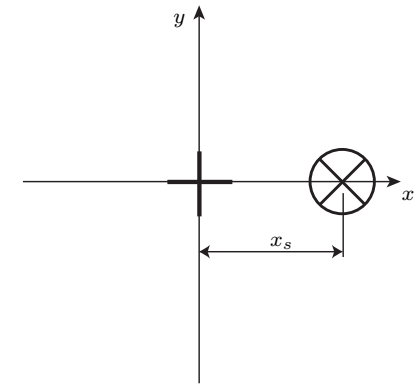
The case with a purely dynamic eccentricity is more complex to describe. In this case, the following conditions apply to Fig. 1b:

- The axis of rotation of the rotor (marked as x in the figure) coincides with the geometric centre of the stator bore (marked as $+$ in the figure);
- The axis of rotation of the rotor is displaced by a dynamic offset vector from the geometric centre of the rotor;
- The geometric centre of the rotor (marked as o in the figure) orbits around the geometric centre of the stator bore;
- The geometry is invariant with position along the machine axis.

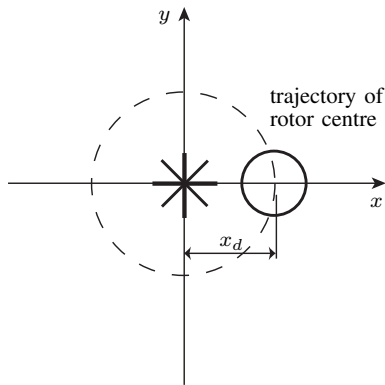
For a purely dynamic eccentricity say of dynamic offset vector $(-x_d, 0)$, at time $t = 0$ the geometric centre of the rotor is displaced by a distance of $+x_d$ from the geometric centre of the stator bore. The axis of rotation of the rotor remains concentric with the stator bore and is displaced by a distance $-x_d$ in the x -direction at the same time instant $t = 0$ from the geometric centre of the rotor. As the rotor revolves, the geometric centre of the rotor traces out a circular path which is concentric with the geometric centre of the stator bore. This circular path is shown by the dotted circle in Fig. 1b.

A 10 % eccentricity value or ratio was used in this paper in the purely static and purely dynamic eccentricities simulations since manufacturers tend to limit the amount of eccentricity to this value [15]. This 10 % eccentricity value or ratio for the generator studied in this article is taken of the mean air-gap length given in Table I. Of importance is to note that rotors in hydropower generators are normally short and fat as opposed to long rotors used in turbo-generators.

There can be various reasons for the occurrence of rotor whirling as was briefly discussed in the introductory section. Mass eccentricity that entails unbalance only gives rise to synchronous whirling. This paper however is going beyond the usual simplification in literature that whirling solely refers to synchronous (forward) whirling. In a hydropower machine, the UMP and whirling mutually influence each other. This mutual effect can be too complex to model in a FEM-based EM software product. This issue is re-visited in the second paragraph in Section III-C. That being said, the UMP can be viewed as one factor that causes dynamic eccentricity and hence whirling since the radial UMP always tends to pull the rotor towards the stator bore inner surface, causing the rotor to bend. Another factor that can give rise to



(a) Purely static eccentricity in the x -direction



(b) Purely dynamic eccentricity

Fig. 1. The different eccentricity motion types explored in this paper are shown. Fig. 1a portrays a purely static eccentricity in the positive x -direction whereas Fig. 1b depicts the case of a purely dynamic eccentricity with the rotor centre taking the dotted path. The rotor geometric centre o is initially placed at the point $(x_d, 0)$. For the meaning of the symbols x , o and $+$, see text

the phenomenon of whirling in hydropower generators is the effect of the water hitting the turbines' blades that are fixed at the bottom of the rotor shaft. This external forcing due to the water brings about more play in the bearings that support the generator rotor, hence imparting whirling motion as well. A further example of a cause of whirling is an initially bent rotor taking the form of a circular arc between the bearings holding the generator rotor.

For the alternator under study, the direction of rotation of the rotor is counterclockwise viewing from above. This implies that with a positive whirling, the whirling takes place in the same direction as the rotating rotor and the path taken by the moving centre of the rotor then follows an anticlockwise direction along the dotted trajectory of Fig. 1b in the purely dynamic eccentricity motion. An explanation of having a whirling speed other than the synchronous mechanical angular velocity of the rotor, ω_{ro} , is in place here when considering a purely dynamic eccentricity motion. In particular, with the case of forward synchronous whirling i.e. when the whirling velocity has the same speed as ω_{ro} and the rotor is whirling in the same direction as the rotor spin, after one full revolution of the path that the geometric centre of the rotor takes, a fixed point on the rotor other than the latter's geometric centre has also undergone a similar full revolution. In other words, a cycle of whirling takes the same amount of time that the fixed point of the rotor takes to make one complete revolution. The case of non-synchronous whirling for a purely dynamic eccentricity motion in an EM analysis is rarely treated in the literature according

to the best knowledge of the authors. For the situation where there is whirling in the backward direction with a whirling speed say two times the speed ω_{ro} of the rotor, this means that a cycle of whirling takes half the amount of time that the aforementioned fixed point of the rotor takes to make one complete revolution. Put differently, the geometric centre of the rotor is moving much faster with twice the corresponding speed of ω_{ro} in the backward direction as opposed to the rotor that is rotating in the forward direction with a speed of ω_{ro} .

Fig. 1b also shows that there is just one whirl velocity component since we only have two points that are in relative motion with each other (in a two-dimensional frame). These two points are firstly the moving rotor centre on the dotted trajectory and secondly the fixed stator bore centre at $(0, 0)$. We have a constant whirling velocity since the magnitude of the dynamic offset vector that represents the eccentricity value or ratio is constant and the rotation velocity of the rotor geometric centre is uniform along the dotted trajectory.

III. THE GENERATOR MODEL

A. Physical parameters of the generator unit

A two-dimensional model of the rotor and the stator of the generator was considered sufficient for the modelling on the computer as skewing effect(s) of the rotor is(are) not accounted for. Thus the eccentricities and geometries considered are independent of the axial Cartesian direction z . The main parameters of the 185 kW 3-phase salient-pole type alternator that are useful in the simulations are given in Table I. The rotor poles sit outwards on the rotor rim which in turn is fixed on the spider. This is shown in Fig. 2. It is to be noted at this stage that the simulations in this article were carried out using the full two-dimensional model of the generator and not with just the one-pole pitch model as shown in Fig. 2 as eccentricity destroys any spatial periodicity in the EM model(s).

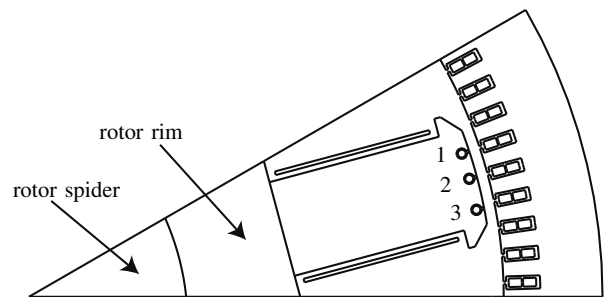


Fig. 2. Fig. shows the cross section of one EM model of the generator studied for one pole pitch only and when there is no eccentricity. The solid rotor rim sits on the solid spider. The uneven spatial distribution of the three damper bar slots on a pole shoe can also be seen. The two damper bars Bars 1 and 3 on every pole shoe are in an asymmetric configuration around the centre damper slot that holds Bar 2. More explicitly, if a line is drawn from the rotor geometric centre through the centre damper slot, then the angle subtended by the line from the rotor centre through the damper slot for Bar 3 is greater than the corresponding angle subtended for the damper slot with Bar 1 considered instead. In the simulations, the direction of rotation of the rotor is anticlockwise with Bar 1 leading. The damper bar slots are open at the top of the pole shoe

All the simulations in this paper are for the no-load case. This was preferred to the load condition since measurements are easier to do when currents are not flowing in the stator coils. Also, vibrations that appear when the generator is operating under a no-load condition may be masked once the stator terminals start supplying current to a load source.

TABLE I. Important dimensions and parameters of the generator

Parameter	Value
Rotor axial length [mm]	305
Rotor spider radius, [mm]	120.1
Rotor rim external radius [mm]	200.1
Rotor external radius ¹ [mm]	354.1
Mean air-gap length, [mm]	8.4
Mechanical angular velocity, ω_{ro} [rad/s]	52.36
Number of poles	12
Number of stator slots	108

¹ This includes the pole shoe height

B. The eddy current problem in a generator

In any electrical machine, there are regions which are conducting and regions which are not conducting in regard to eddy current presence [16]. If we write the Maxwell's Equations with respect to the fixed stator reference frame, then we have [17]

$$\begin{aligned}\nabla \times \mathbf{H} &= \mathbf{J} \\ \nabla \times \mathbf{E} &= -\frac{\partial \mathbf{B}}{\partial t} \\ \nabla \cdot \mathbf{D} &= \rho_V \\ \nabla \cdot \mathbf{B} &= 0\end{aligned}\quad (1)$$

where

$$\mathbf{J} = \begin{cases} \mathbf{J}_0 & \text{in } \Omega_n \\ \sigma(\mathbf{E} + \mathbf{v}_{ro} \times \mathbf{B}) & \text{in } \Omega_c \end{cases}\quad (2)$$

In Equation (2), the region Ω_n refers to the non-conducting domain with boundary Γ_n and Ω_c refers to the eddy current conducting domain with Γ_c as its boundary respectively. A solution to the magnetic field in the whole domain $\Omega_n \cup \Omega_c$ only becomes possible when the coupling that exists at the interface(s) between the separate regions in terms of the continuity of $\mathbf{H} \times \mathbf{n}$ and $\mathbf{B} \cdot \mathbf{n}$ is maintained and the constitutive equations of matter are introduced as well. For a two-dimensional setting, a generator will have a magnetic vector potential A_z and current density J_z . Equations (1) and (2) can then be cast together as

$$-\frac{\partial^2 A_z}{\partial x^2} - \frac{\partial^2 A_z}{\partial y^2} = \mu J_z\quad (3)$$

and

$$-\frac{\partial^2 A_z}{\partial x^2} - \frac{\partial^2 A_z}{\partial y^2} = -\sigma \mu \frac{\partial A_z}{\partial t} + \sigma \mu \left(\mathbf{v}_{ro} \times \left[\frac{\partial A_z}{\partial y} - \frac{\partial A_z}{\partial x} \right] \right)\quad (4)$$

with the boundary condition as $A_z = 0$ on the stator yoke of the generator. A list of common assumptions governing Maxwell's equations as applied to electrical machines is listed in [18], [19].

Whirling term(s) is(are) not seen in Equations (3–4). This is because the FEM-based EM software product, MagNet [20], that is used accounts for the effect(s) of whirling in the modelling process and the user does not have access to the field equations being solved. By allowing multiple degrees of freedom to be set on the rotor with different motion components, the effect(s) of rotor whirling come(s) into being by relative motion between the geometric centre of the rotor and an axis of rotation of the rotor in the modelling stage. This axis of rotation in a purely static eccentricity as shown in Fig. 1a is at a fixed point $(x_s, 0)$ and for the case of a purely dynamic eccentricity is at the centre of the stator bore at the point $(0, 0)$ as displayed in Fig. 1b.

C. Parameters used in the simulations

For all the simulations, the EM model was set up with no running up of the rotor. In other words, the speed of the rotor was at its synchronous value right from the start of the simulations and this

remains so till the end of the simulations. Moreover, the model makes all current sources to be on at the onset of the simulations. The time step in the transient simulations had a value of 0.1 ms and it took 120 ms of simulation time for a fixed point on the rotor to make one complete revolution (see also Table II). For the eccentric motion simulations, the initial position of the rotor has been set to lie on the positive side of the Cartesian x -axis.

The two types of eccentricities that are covered in this article have been examined in Section II. As regard to the purely static eccentricity simulations, ten revolutions of the rotor were deemed necessary before steady state operation was reached. The steady state condition in the EM simulations can be gauged for instance by waiting for when the ohmic losses in the rotor rim stabilise. As for the purely dynamic eccentricity simulations, three rotor revolutions were prescribed irrespective of the whirling velocity and whirling direction that the rotor takes. It is to be expected that as the rotor whirls, the flux densities on the rotor vary as well which in turn affect the whirling velocity of the rotor. This additional complexity was not introduced in the model. The rotor has been set to whirl with a constant whirling velocity for the whole duration of the simulations. The goal with such a simulation type is to find the steady state field solutions corresponding to a particular whirling frequency.

Different whirling speeds have been considered in the simulations within a range of six times the synchronous velocity (or the rotor mechanical angular velocity) of $\omega_{ro} = 52.36$ rad/s both in the positive and in the negative whirl directions. This wide whirling frequencies span was considered suitable subject to a reasonable amount of computation time that it requires and of course it can be enlarged or decreased if desired. The range of whirling frequencies considered may be viewed as excessively wide. However, it is to be remarked that in the general case where a combination of purely static eccentricity and a purely dynamic eccentricity exists, then the whirling frequency may expect to vary by large amounts depending upon the static and dynamic eccentricity ratios therein. With mixed eccentricities motion, the whirling frequency of the moving geometric centre of the rotor with respect to the fixed stator bore centre becomes non-constant while the local whirling frequency, with respect to the axis of rotation at coordinates $(x_s, 0)$, due to the dynamic eccentricity component is still constant. So while considering a wide whirling ratio range $-6.0 \leq \omega_{whr} \leq 6.0$ in the purely dynamic eccentricity simulations may appear superfluous and not possibly be observed in practice, it is to be emphasised that mixed eccentricities motion reflects better the motion of a hydropower rotor and in this case the whirling ratios embrace a wide range of whirling frequencies. Hence, examining a wide ω_{whr} range as done in this paper is relevant as this wide range gives valuable information of the effect(s) of what a more accurate whirling behaviour due to mixed eccentricities motion can bring. A subset of whirling velocities have been picked to illustrate the results and these whirling frequencies are given in Table II. Halfway whirling ratio values of the extremum whirling ratios of -6.0 and 6.0 which are at $\omega_{whr} = -3.0$ and 3.0 respectively are proper choices to study.

Furthermore, in all the three sets of simulations for the no eccentricity case, the purely static eccentricity case and the purely dynamic eccentricity case, the magnetomotive force of the field windings was constant at 2430 A–turns. Also, the damper bars, which are made of copper, were connected in a circuit as a squirrel cage with interconnections between poles.

IV. RESULTS AND ANALYSIS

A. Force on the rotor

In this section, the forces acting on the rotor are presented for different cases, namely first for an ideal case without any rotor-stator eccentricity, secondly for a rotor that is statically eccentric at 10 %

TABLE II. Whirling speeds used in the simulations

Whirling ratio, ω_{whr}	Whirling speed, ω_{wh} [deg/s] ^a	Whirling speed, ω_{wh} [rad/s]
-6.0	-18 000	-314.16
-3.0	-9 000	-157.08
1.0 ^b	3 000	52.36
3.0	9 000	157.08
6.0	18 000	314.16

^a This unit can be conveniently set within MagNet [20]

^b This value represents (forward) synchronous whirl and has been included in the table to give an idea of the magnitudes of the whirling speeds used in the simulations

ratio in the x -direction and thirdly for a rotor that undergoes a purely dynamic eccentricity motion with 10 % offset or eccentricity ratio. For the latter case, the whirling speeds as listed in Table II are considered. MagNet [20] computes the forces acting on the rotor through the latter's centre of mass. For the rotor under study that is assumed to be homogeneous and that has a perfectly circular structure, this centre of mass coincides with the geometric centre of the rotor.

Fig. 3 next shows the time histories of the forces in the Cartesian x -direction for the case with no eccentricity and for the case with a static eccentricity of 10 % in the positive x -direction respectively. Furthermore, Fig. 4 shows the variations of the forces in the Cartesian x -direction over time for some different whirling frequencies. In addition, estimates of the spectrum contents for each of the force curves of Fig. 4 have been provided in Fig. 5. While the objective with the spectrum estimates is the identification of the frequency contents of the signals, the tonal components have been scaled as a one-sided RMS-scaled linear spectrum estimates using the Welch method [21]. This non-parametric estimate is given by

$$\hat{X}^{LS}(f_l) = \sqrt{\frac{2}{N_2 N_1 U} \sum_{n_2=0}^{N_2-1} \left| \sum_{n_1=0}^{N_1-1} x_l(n) w(n) e^{-j \frac{2\pi n l}{N_1}} \right|^2}, \quad f_l = \frac{l \cdot f_s}{N_1} \quad (5)$$

where N_1 is the length of one periodogram, N_2 is the number of periodograms, $l = 0, \dots, N_1/2$, f_l is the frequency at index l , f_s is the sampling frequency, $w(n)$ is the data window and

$$U = \frac{1}{N_1} \left(\sum_{n=0}^{N_1-1} w(n) \right)^2 \quad (6)$$

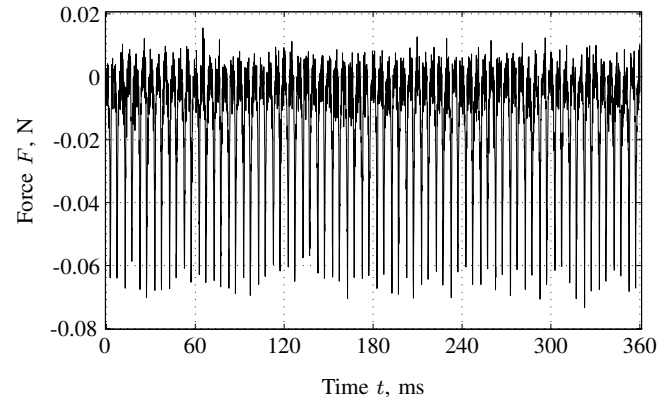
is the window-dependent resolution bandwidth normalisation factor [22] for power spectrum estimation. It is essential to note that the factor of 2 is not used in Equation (5) at index $l = 0$. The selected linear spectrum estimation parameters are shown in Table III. Next, Fig. 6 displays the steady state average UMP in the radial and tangential directions respectively over the whole span of the whirling range of six times the synchronous whirl speed both in the forward and in the backward whirled motion.

TABLE III. Linear spectrum estimation parameters in Equation (5)

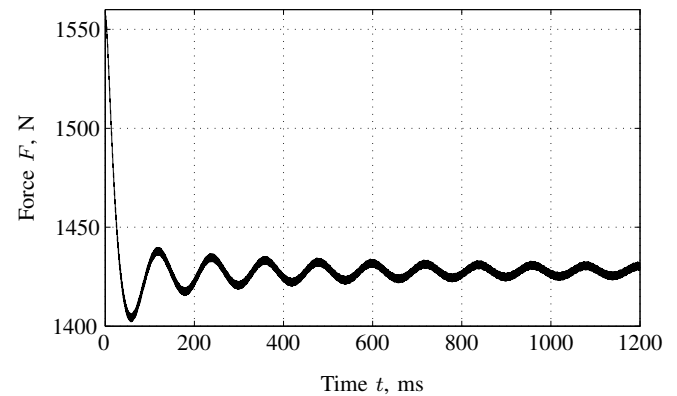
Parameter	Value or name
Data length (samples)	3 201
Sampling frequency, f_s [kHz]	10
Length of periodogram, N_1 (samples)	3 201
Time window, w	Flat top ¹
Number of periodograms, N_2	1

¹ This is the flattopwin window in MATLAB [23]

Two observations can be made from the results presented in this section. Firstly, Figs 4 and 5 show that the whirling frequency dictates the frequency of the force variations. For example, considering Fig. 4c



(a) No rotor-stator eccentricity

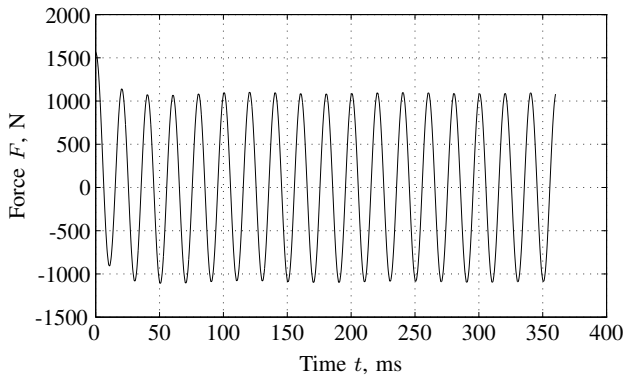


(b) Static eccentricity of 10 %

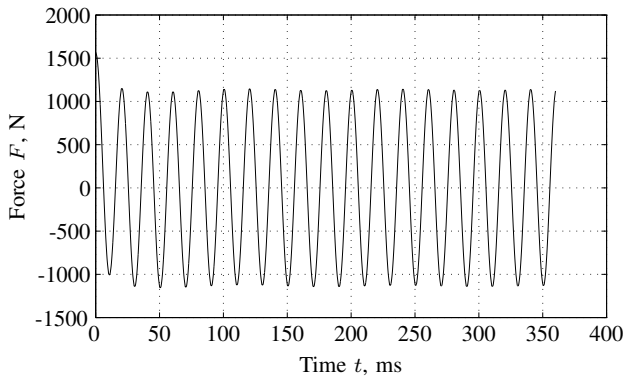
Fig. 3. Time histories of the forces acting on the rotor in the Cartesian x -direction. The result for no eccentricity is shown in Fig. 3a for three rotor revolutions whereas the result for a static eccentricity of 10 % eccentricity ratio of the mean air-gap length in the positive x -direction is shown in Fig. 3b over ten rotor revolutions. Fig. 3b shows that it takes a long simulation time for steady state condition in the force curve to be reached

for a case of whirling ratio $\omega_{whr} = -3.0$, the time period of the sinusoidal force variation is one third of the time for the case of synchronous whirling (not shown in this paper) which gives 40 ms (see also Table II and Section III-C). Secondly, Fig. 6 shows that the UMP components both in the radial and in the tangential directions do not have high magnitudes for the 10 % eccentricity ratio studied. The dampening effect of the damper windings is estimated to be a substantial amount of around 30 % in Fig. 6 for the radial UMP component at high whirling ratios of -6.0 and 6.0 in relative to the magnitude of the radial UMP component at synchronous whirl speed.

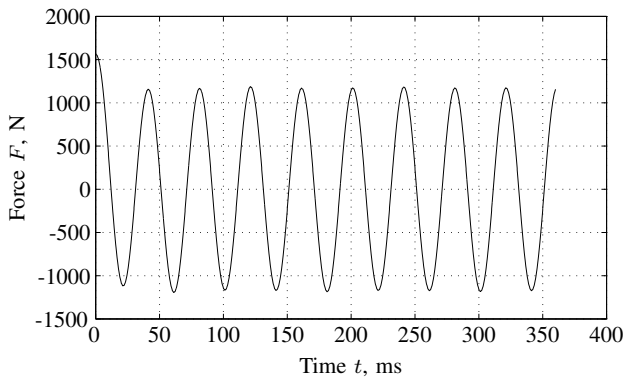
Of importance is to note that force measurements were carried out [14] and it has been reported that a static eccentricity in the x -direction of 24 % gives a horizontal force on the rotor of around 4 kN when no damper windings are present. A corresponding purely static simulation in MagNet [20] gave a comparable answer; This result is not shown in this article. We should however remark that a purely static eccentric rotor is almost impossible to achieve in practice unless both a static and dynamic balancing of the rotor have been properly carried out. No thorough information on the rotor balancing for the generator under study was available though. Besides, as in the case of a purely static eccentricity motion as given in Fig. 3b in the x -direction, the corresponding force curve and spectrum contents are expected to be similar in the Cartesian y -direction as well.



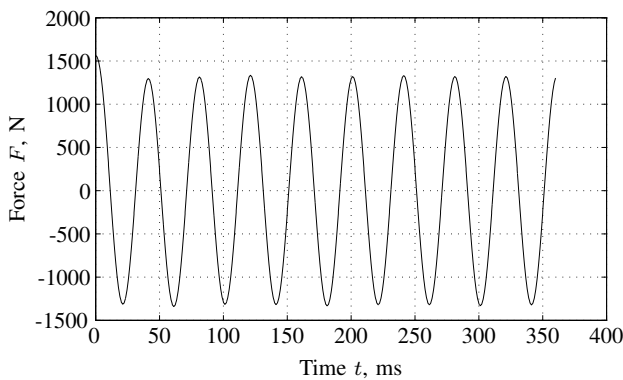
(a) Whirling ratio of -6.0



(b) Whirling ratio of 6.0

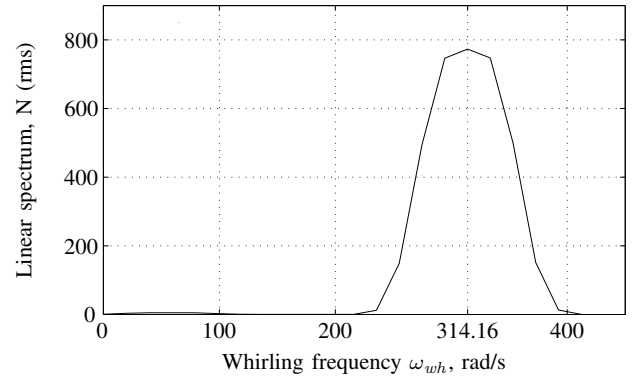


(c) Whirling ratio of -3.0

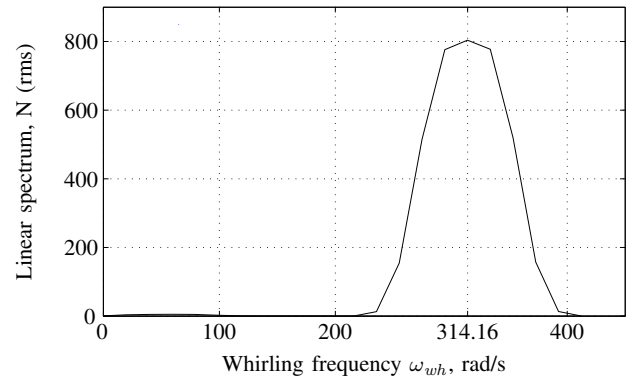


(d) Whirling ratio of 3.0

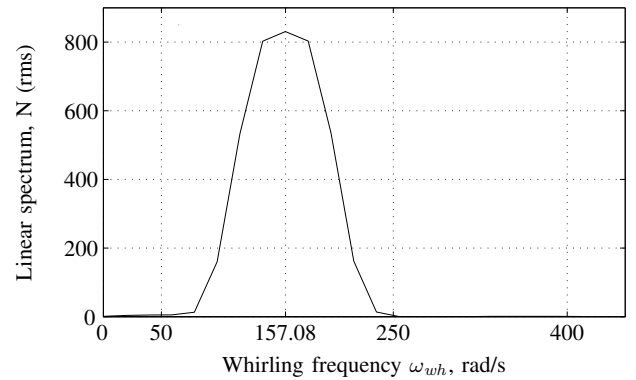
Fig. 4. Time histories of the forces acting on the rotor in the horizontal direction in the case of a purely dynamic eccentricity motion of the rotor of 10 % eccentricity ratio for different whirling ratios namely -6.0, 6.0, -3.0 and 3.0



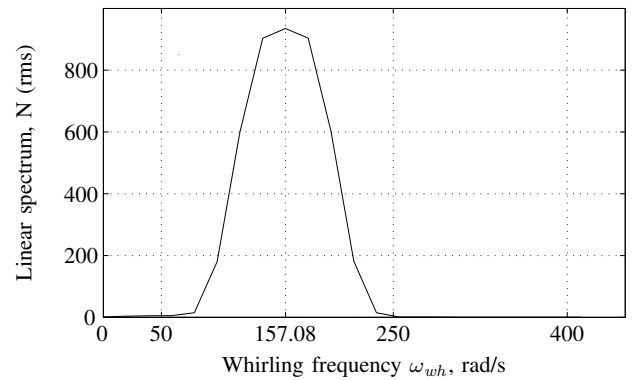
(a) Whirling ratio of -6.0



(b) Whirling ratio of 6.0

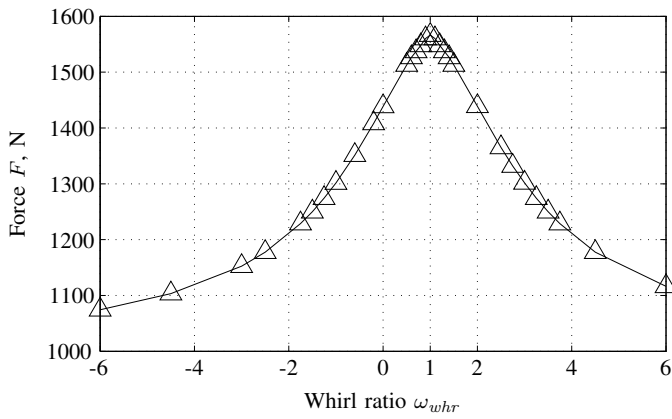


(c) Whirling ratio of -3.0

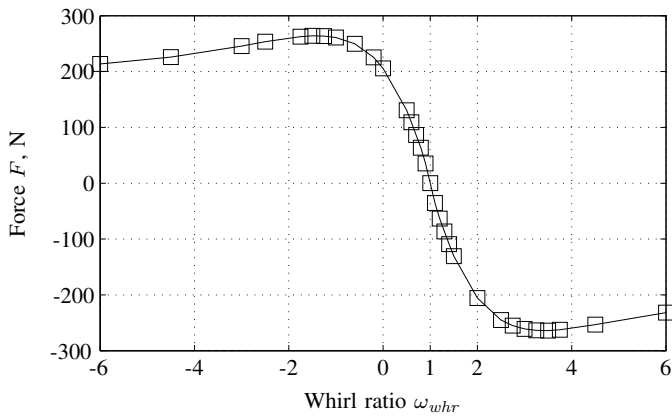


(d) Whirling ratio of 3.0

Fig. 5. One-sided linear spectrum estimates of the force time histories of Fig. 4 in the range 0 rad/s to 400 rad/s (see Table II) for different whirling ratios namely -6.0, 6.0, -3.0 and 3.0. The parameters used in the spectrum analysis are given in Table III. A whirl ratio of unity corresponds to a whirling frequency of 52.36 rad/s



(a) Radial force on the rotor



(b) Tangential force on the rotor

Fig. 6. Radial force and tangential force on the rotor with a purely dynamic eccentricity motion of 10 % eccentricity ratio. The transparent triangles and squares on the graphs depict the whirling frequencies used in the simulations expressed as whirl ratios and the corresponding force values are joined with straight lines. Synchronous whirl is marked on the graph as the point $\omega_{whr} = 1$

B. Flux density distribution and harmonics in the air-gap

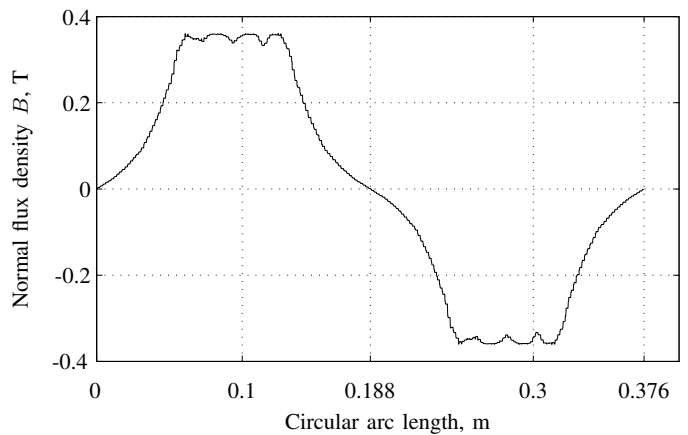
The flux density \mathbf{B} together with the currents flowing in the various parts of the generator, in principle, provide all the information from which any other EM parameter of interest can be derived. Current values and their interpretation are postponed to the next section and this section presents flux density information. A knowledge of \mathbf{B} provides, among other things, information on how much use of the iron is made in the generator and this indirectly tells us whether the size of the generator is right for its power output.

Figs 7 and 8 display the spatial variation of the flux density in the air-gap in the normal direction over two consecutive poles at the last time instant in the simulations for the different motion cases as considered in Section IV-A. The two consecutive poles which were chosen faced the smallest air-gap position. The arc length considered is at a radius of 359 mm (see Table I) which is well into an air-layer in the air-gap where force computations take place and the spatial circular arc length over two consecutive poles amounts to $2 \times 359 \text{ mm} \times \frac{\pi}{6} \approx 376 \text{ mm}$. A spatial resolution of 2048 points exists in Figs 7 and 8.

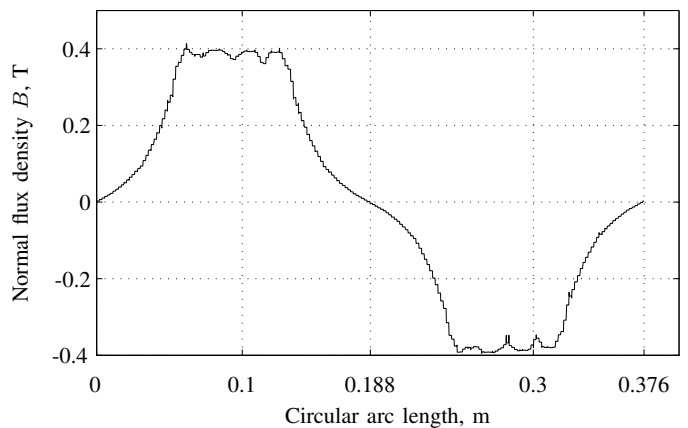
Figs 9 and 10 give the harmonic contents of the spatial variation of the flux density distributions of Figs 7 and 8 respectively. We are interested in the frequency contents in order to view what kinds of frequencies whirling can bring but the amplitude levels are amenable

to comparison as well since the latter are the absolute magnitude values from the Fourier Transform results of the spatial variation of the flux densities. The amplitudes of the peaks in the Fourier Transform estimates have been normalised with the sampling wavenumber which is around 5444.96 m^{-1} .

It is immediately obvious from the flux density estimates in Figs 7 and 8 that the eccentricity we are considering can be small in addition to the generator having perhaps not a small air-gap in relation with the diameters of the rotor and that of the stator (see Table I), and this is causing the flux density behaviours to be practically the same even at very high whirling ratios. In the simulations a maximum value of $B \leq 0.4 \text{ T}$ was noted in all cases and this also explains the relatively low force magnitudes as seen in Section IV-A. At this flux density value, we are perhaps not making use of the whole iron available to us in the generator. This situation can nevertheless be different with a higher eccentricity ratio value.



(a) No rotor-stator eccentricity



(b) Static eccentricity of 10 %

Fig. 7. Spatial distribution of the normal flux density in the air-gap over a pole pair for the case of no rotor stator eccentricity in Fig. 7a and for the case with a purely static eccentricity ratio of 10 % of the mean air-gap length in the positive x -direction in Fig. 7b. A circular length of around 188 mm subtends an angle of 30° mechanical for one pole pitch

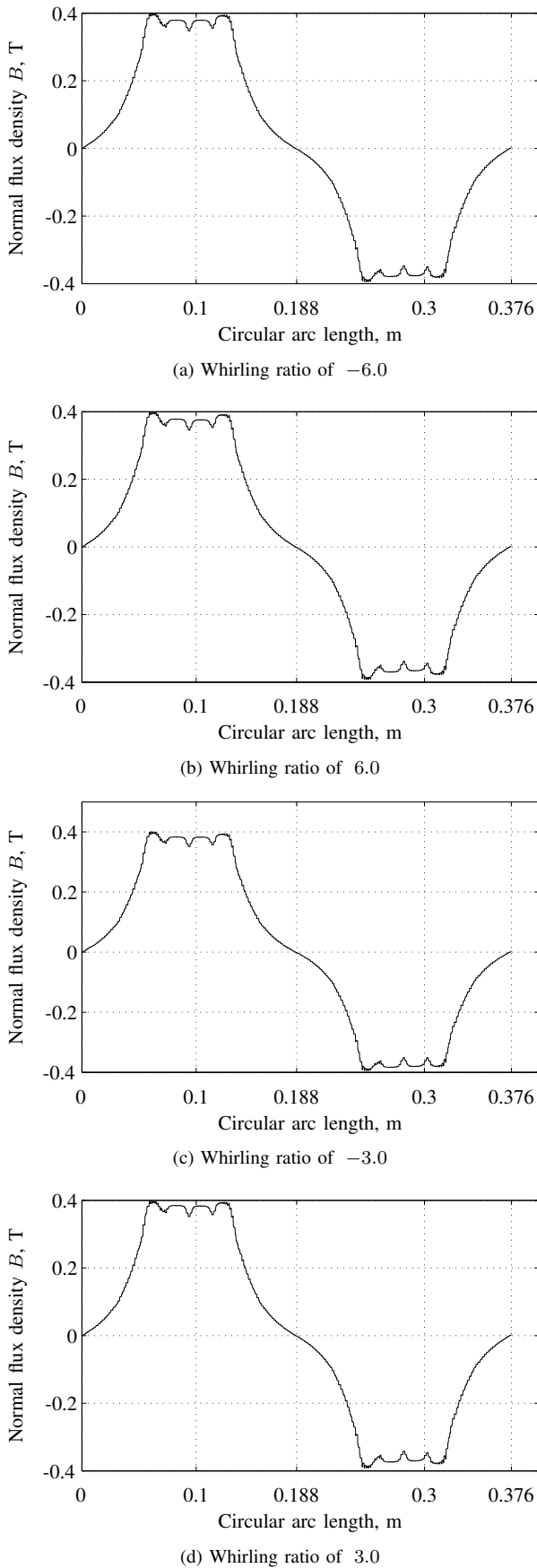


Fig. 8. Spatial distribution of the normal flux density in the air-gap over a pole pair for different whirling ratios namely -6.0, 6.0, -3.0 and 3.0. The motion type is a purely dynamic eccentric motion of the rotor of 10 % eccentricity ratio of the mean air-gap length. A circular length of around 188 mm subtends an angle of 30° mechanical for one pole pitch

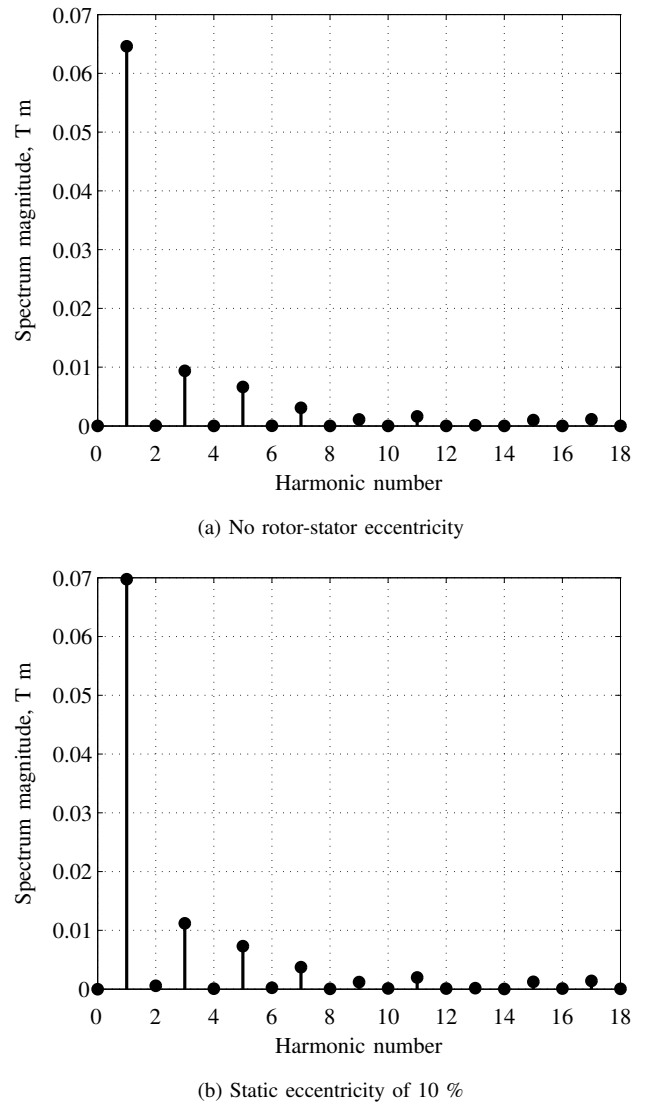


Fig. 9. Flux density spatial spectrum estimates stem plots as a function of harmonic number showing the first eighteen harmonics for the case of no rotor stator eccentricity in Fig. 9a and for the case with a purely static eccentricity ratio of 10 % of the mean air-gap length in the x -direction in Fig. 9b. The amplitudes of the spectrum estimates represent absolute magnitude values from the Fourier Transform computation that have been scaled down by the sampling wavenumber. Refer also to Fig. 7 for the flux density spatial variation

C. Maximum currents in the damper bars and in the rotor rim

Induced currents, whether desirable or undesirable, exist in any generator. Damper bars allow the flow of currents in order to minimise oscillations of the rotor and this is a desirable feature. On the other hand, induced currents flow for example in the solid rotor rim on which the poles lie and this is undesirable. While the solid rotor rim and the solid spider on which the former is fixed have been modelled with the same electrical resistivity value, only the conducting rotor rim will be considered here as the eddy currents affect the solid rim considerably more than the solid spider since the latter is much further away from the poles (see also Fig. 2). The pole shoes and the stator materials are laminated and hence do not have induced currents.

The roles and importance of the damper bars have been documented in the literature [1], [24]. For an alternator standing alone, pole slipping is not an issue and as mentioned in Section III-C, the rotor speed ω_{ro} is kept at its synchronous value (see Table I) irrespective

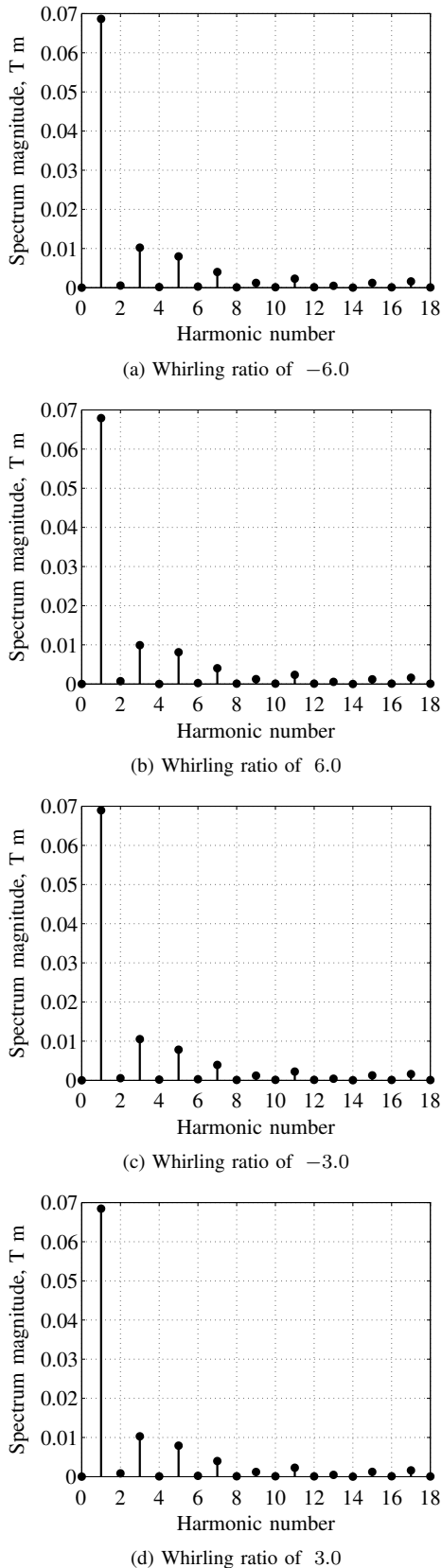


Fig. 10. Flux density spatial spectrum estimates stem plots as a function of harmonic number for different whirling ratios namely -6.0, 6.0, -3.0 and 3.0 showing the first eighteen harmonics. The motion type is a purely dynamic eccentric motion of the rotor of 10 % eccentricity ratio of the mean air-gap length. The amplitudes of the spectrum estimates represent absolute magnitude values from the Fourier Transform computation that have been scaled down by the sampling wavenumber. Refer also to Fig. 8 for the flux density spatial variation

of the whirling speed ω_{wh} used in Table II. The problem of having a high current flow can be immediately linked to heat dissipation in the machine, depending also on the resistivity of the material. It is to be noted that vents and cooling ducts were not modelled in the EM analysis since these geometric features will only require finer mesh densities in the finite element analysis, which would increase the solver time. The electrical resistivities of the conducting rim and those of the damper bars were 5×10^{-7} ohm-m and 2.092×10^{-8} ohm-m respectively.

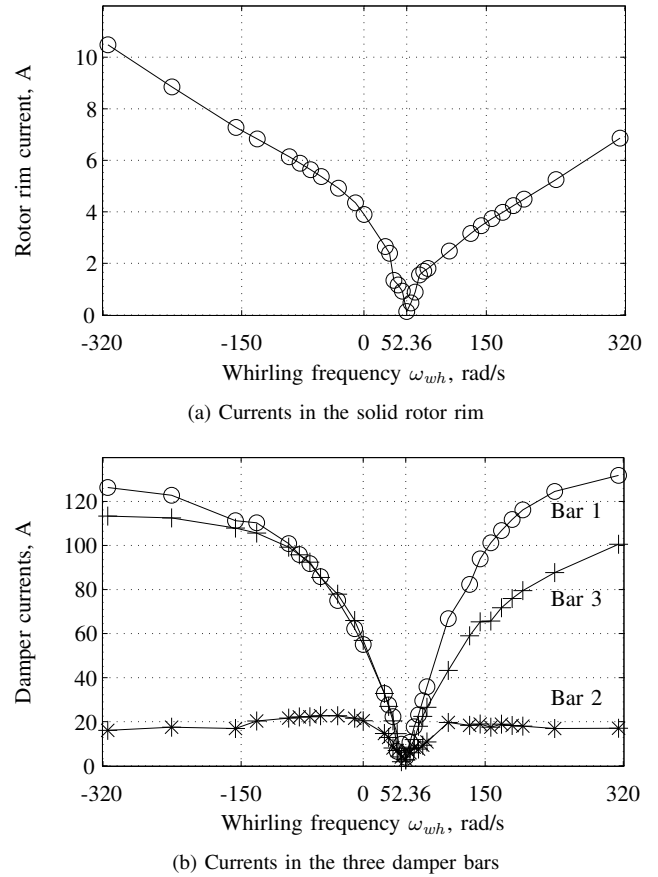


Fig. 11. Fig. 11a shows the maximum induced current flowing into the solid rotor rim while Fig. 11b presents the maximum damper currents flowing in the damper bars. The currents are for one pole only and the pole chosen is the one that adjoins the minimum air-gap length. The range of whirling frequencies considered is in the whirling ratio range of -6.0 to 6.0. Synchronous whirl is marked on the graph as the point $\omega_{wh} = 52.36$ rad/s (see also Table II). The arrangement of the damper bars, Bars 1 to 3, is according to the schematic shown in Fig. 2. The case for static eccentricity of 10 % can be read from the plots at the value $\omega_{wh} = 0$ rad/s

Fig. 11 presents the maximum currents flowing in the damper bars and in the rotor rim for one pole that adjoins the minimum air-gap length. The currents' variations have tonal components, and Fig. 11a and 11b shows the peak values of these sinusoidal time series. Visual inspection of Fig. 11 reveals that the currents can increase to very high levels (see Fig. 11b) when there is rotor whirling, be it in the forward or in the reverse whirl direction. A high current level can break down the insulation surrounding the damper bar. It is to be noted that in the simulations, information pertaining to the insulation type and material was not available. The level of currents in the rotor rim is not high and this can be attributed to the fact that the rim is recessed away from the air-gap. Besides, we can note that forward synchronous whirling at $\omega_{wh} = 52.36$ rad/s produces the least current flow and this whirling case is more common in hydropower

generators. Synchronous (forward) whirling can be associated to a stable operating condition of a hydropower generator as was seen in an earlier work by two of the authors [13].

On a machine without rotor eccentricity, it has been found that a current of about 0.02 A and currents of around 1 A were flowing in the solid rotor rim and damper bars respectively. These low currents are expected in a machine with perfectly centred rotor and stator. This provides a useful check for the EM models used in the simulations. It is thought that the centre damper bar has the smallest current produced by the whirling due to the fact that the outer damper bars (see Fig. 11b) act as shields [19].

D. Ohmic losses in the rotor rim

In solid materials, power losses are dissipated. In the model, only a few parts are electrically conducting and the stator material together with the pole shoes material are modelled with zero electrical conductivity. Since the poles sit outside on the rim, the magnetic diffusion of the magnetic field into the rim is small with a low value of the flux density and ohmic losses appear almost instantaneously at switch-on time without any considerable magnetic diffusion time. Ohmic losses in the damper bars and in the rotor rim are expected to have the same behaviours as in Fig. 11 from Section IV-C. In MagNet [20], the ohmic loss calculations for solid conductors neglect the hysteresis loss component. Table IV presents time average ohmic losses due to the eddy currents for some whirling cases as considered in this paper.

TABLE IV. Time average ohmic losses in the complete rotor rim structure for different whirling frequencies in the purely dynamic eccentricity motion cases

Whirling ratio	Whirling speed [rad/s]	Ohmic loss, [W]
-6.0	-314.16	27.828
-3.0	-157.08	10.908
3.0	157.08	3.720
6.0	314.16	15.672

Backward whirling is seen to produce considerably higher eddy current losses in the rotor rim than the corresponding forward whirling speeds do. It is also noted that the ohmic losses are very low. Low flux density values as observed in Section IV-B together with the outwards geometric configuration of the rotor poles (see Fig. 2) are the causes for such low ohmic losses. As expected, the ohmic losses are practically nil for the case without any eccentricity with a loss value of about 0.08 W (not included in the results of Table IV).

V. CONCLUSIONS

This paper aimed at bridging the gap between what electrical engineers usually want from EM simulations and what mechanical engineers would like to see. In this respect, whirling dependent behaviours of the rotor motion for a purely static eccentricity case and for a purely dynamic eccentricity case have been studied. The effects of whirling from a mechanical point of view were earlier treated by two of the authors [12], [13]. The present article serves to illustrate the importance of whirling but from an electrical engineering perspective. A hydropower machine is complex to model as there are so many variables that come into play and any artificial schism between the two above-mentioned engineering fields can only be eliminated when the generator is not viewed as an isolated item but instead as one which is under the influence of other parts in motion in a hydropower machine. MagNet [20], by being a general purpose FEM-based EM field modelling software product, allows a body to have several degrees of freedom and hence this advantage was taken of when building the necessary models in this paper.

Perhaps due to the large air-gap length that is providing high reluctance in the magnetic circuit, the results presented in this paper tend to have low order of magnitudes and no drastic changes in the force or in the flux density magnitudes for instance have been noted in the simulations. Higher eccentricity values other than the studied 10 % were not considered as they do not occur in a generator when under normal operating conditions. It has also been seen (see Fig. 6) that the effect of the damper bars become pronounced on the force magnitudes at large whirling ratios. In addition, it has been found that backward whirling tends to induce higher eddy currents than forward whirling does. The very low ohmic losses in the rotor rim also represent a key finding in this paper. A no-load model is considered sufficient though it can be argued that the (radial) UMP magnitudes may decrease when there is load. That said, the objective of this paper was not to compare the effect of a loaded versus an unloaded generator but to see how whirling affects important EM parameters that are normally used by electrical engineers.

A new contribution to the field of EM analysis of hydropower generators is the treatment of non-synchronous whirling in this paper and demonstration of its effect(s) on some EM parameters. This new addition has been combined with common eccentricity types that are reported in the literature.

ACKNOWLEDGMENTS

This project has been sponsored by Svenskt VattenkraftCentrum (SVC) in Sweden. The main author wishes to express his sincere thanks to the MagNet's Support team at Infolytica Europe. Information regarding the generator has been supplied by Dr Urban Lundin from Uppsala Universitet, Sweden.

REFERENCES

- [1] M. Walker. *Specification and Design of Dynamo-Electric Machinery*. Longmans' Electrical Engineering Series, 1915.
- [2] E. Rosenberg. Magnetic pull in electrical machines. *Transactions of the American Institute of Electrical Engineers*, 37(2):1425–1469, 1918.
- [3] I. Ozelgin. Analysis of magnetic flux density for airgap eccentricity and bearing faults. *International Journal of Systems Applications, Engineering & Development*, 4(2):162–169, 2008.
- [4] D. de Canha, W.A. Cronje, A.S. Meyer, and S.J. Hoffe. Methods for diagnosing static eccentricity in a synchronous 2 pole generator. In *Power Tech, IEEE, Lausanne*, pages 2162–2167, July 2007.
- [5] I. Tabatabaei, J. Faiz, H. Lesani, and M.T. Nabavi-Razavi. Modeling and simulation of a salient-pole synchronous generator with dynamic eccentricity using modified winding function theory. *IEEE Transactions on Magnetics*, 40(3):1550–1555, May 2004.
- [6] G. Joksimovic and C. Bruzzese. Static eccentricity detection in synchronous generators by field current and stator voltage signature analysis—Part I: Theory. In *Electrical Machines (ICEM), XIX International Conference. 6–8 September, Rome, Italy*, pages 1–6, 2010.
- [7] B.A.T. Iamamura, Y. Le Menach, A. Tounzi, N. Sadowski, and E. Guillot. Study of static and dynamic eccentricities of a synchronous generator using 3-D FEM. *IEEE Transactions on Magnetics*, 46(8):3516–3519, August 2010.
- [8] J. Faiz, M. Babaei, J. Nazarzadeh, B.M. Ebrahimi, and S. Amini. Time-stepping finite-element analysis of dynamic eccentricity fault in a three-phase salient pole synchronous generator. *Progress in Electromagnetics Research B*, 20:263–284, 2010.
- [9] T.P. Holopainen, A. Tenhunen, E. Lantto, and A. Arkkio. Unbalanced magnetic pull induced by arbitrary eccentric motion of cage rotor in transient operation. Part 1: Analytical model. *Electrical Engineering*, 88(1):13–24, April 2005.
- [10] T.P. Holopainen, A. Tenhunen, E. Lantto, and A. Arkkio. Unbalanced magnetic pull induced by arbitrary eccentric motion of cage rotor in transient operation. Part 2: Verification and numerical parameter estimation. *Electrical Engineering*, 88(1):25–34, March 2005.
- [11] N.L.P. Lundström and J.-O. Aidanpää. Whirling frequencies and amplitudes due to deviations of generator shape. *International Journal of Non-Linear Mechanics*, 43(9):933–940, November 2008.
- [12] Y. Calleecharan and J.-O. Aidanpää. Dynamics of an hydropower generator subjected to unbalanced magnetic pull. *Proceedings of the Institution of Mechanical Engineers, Part C: Journal of Mechanical Engineering Science*, 225(9):2076–2088, 2011.

- [13] Y. Calleecharan and J.-O. Aidanpää. Stability analysis of an hydropower generator subjected to unbalanced magnetic pull. *IET Sci. Meas. Technol.*, 5(6):231–243, November 2011.
- [14] Division for Electricity, The Ångström Laboratory, Uppsala Universitet, Sweden.
- [15] H. Torkaman and E. Afjei. Magnetostatic field analysis regarding the effects of dynamic eccentricity in switched reluctance motor. *Progress in Electromagnetics Research M*, 8:163–180, 2009.
- [16] O. Biro. Computational Electromagnetics (CEM) Conference 2011—Review of Eddy current analysis. [online]. <http://tv.theiet.org/technology/electronics/10890.cfm>.
- [17] D. Marcsa and M. Kuczmann. Finite element analysis of single-phase induction motors. COMSOL Conference, Budapest, Hungary November 24, pp. 1–6, 2008.
- [18] M.V.K. Chari and P. Silvester. Analysis of turboalternator magnetic fields by finite elements. *IEEE Transactions on Power Apparatus and Systems*, PAS-90(2):454–464, March 1971.
- [19] J.R. Brauer. *Magnetic Actuators and Sensors*. Wiley-IEEE Press, 1st edition, February 2006.
- [20] MagNet, Infolytica Corporation, Montréal, Québec, Canada, 2011, Version 7.1.3.
- [21] W.A. Gardner. *Statistical Spectral Analysis: A Non-Probabilistic Theory*. Prentice Hall, January 1988.
- [22] F. Harris. On the use of windows for harmonic analysis with the discrete Fourier transform. In *Proc. of the IEEE*, volume 66, pages 51–83, 1978.
- [23] MATLAB, The MathWorks Inc., Natick, Massachusetts, USA, 2012, Version 7.14.0.739 (R2012a).
- [24] E.W. Kimbark. *Power System Stability Volume III: Synchronous Machines*, IEEE Press Series on Power Engineering. Piscataway, NJ (Wiley IEEE Press, New York), February 1995.

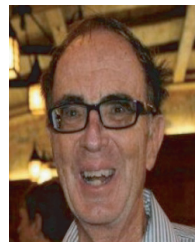
BIOGRAPHIES



Yogeshwarsing Calleecharan received the B.Eng. degree in Mechanical Engineering from the University of Mauritius, Mauritius, in 2000, the M.Sc. degree in Mechanical Engineering from Blekinge Tekniska Högskola, Sweden, in 2003, and the Ph.D. degree in Solid Mechanics from Luleå Tekniska Universitet, Sweden, in 2013. Since 2014 he is a lecturer with the Mechanical and Production Engineering Department, University of Mauritius, Mauritius. His research interests include electromechanics, vibrations and signal analysis, and software development with the Ada programming language.



Jan-Olov Aidanpää received the M.S. degree in Mechanical Engineering from Luleå Tekniska Universitet (LTU), Sweden, in 1987, and the Ph.D. degree in Solid Mechanics from LTU in 1995. Since 2013 he is working as Chair Professor in Computer Aided Design at Luleå Tekniska Universitet, Sweden. His research interest is within non-linear rotor dynamics where he develops measuring techniques and models of hydro and wind power systems.



John R. Brauer earned a bachelor's degree from Marquette University, USA, and master's and Ph.D. degrees from the University of Wisconsin-Madison, USA, all in electrical engineering. He performed engineering research for A. O. Smith Corporation, MSC Software, and Ansoft Corporation, specializing in finite element analysis of electromagnetic devices. He has been Adjunct Professor at Milwaukee School of Engineering, USA, since 1998, and has served as an officer in several professional associations, including the IEEE, where he is a Life Fellow. His publications include over 160 papers and several books. His most recent book is *Magnetic Actuators and Sensors*, 2nd edition, published in 2014 by Wiley IEEE Press.